metals

Article

A New Phenomenological Model to Predict Forming Limit Curves from Tensile Properties for Hot-Rolled Steel Sheets

Wei-Jin Chen [1,2,3], Hong-Wu Song [1,2,*], Shuai-Feng Chen [1,2], Yong Xu [1,2], Si-Ying Deng [1,2], Zheng Cai [3], Xin-Hua Pei [3] and Shi-Hong Zhang [1,2]

1 Shi-Changxu Innovation Center for Advanced Materials, Institute of Metal Research, Chinese Academy of Sciences, Shenyang 110016, China; wjchen16b@imr.ac.cn (W.-J.C.); chensf@imr.ac.cn (S.-F.C.); yxu@imr.ac.cn (Y.X.); sydeng@imr.ac.cn (S.-Y.D.); shzhang@imr.ac.cn (S.-H.Z.)
2 School of Materials Science and Engineering, University of Science and Technology of China, Shenyang 110016, China
3 Research Institute, Baoshan Iron and Steel Co., Ltd., Shanghai 201999, China; zhengcai@baosteel.com (Z.C.); peixinhua@baosteel.com (X.-H.P.)
* Correspondence: hwsong@imr.ac.cn; Tel.: +86-024-83970203

Abstract: A phenomenological model for the prediction of the forming limit curve (FLC) based on basic mechanical properties through a uniaxial tensile test can tremendously shorten the design time of the forming process and reduce the measuring costs. In this paper, a novel phenomenological model named the IMR-Baosteel model (abbreviated as the IB model) is proposed for efficient and accurate FLC prediction of hot-rolled steel sheets featuring distinct variations in thickness and mechanical properties. With a systematic test of the plane strain forming limit (FLC_0), it was found that a higher regression correlation exists between the FLC_0 and the total elongation under different sheet thicknesses. For accurate assessment of the FLC_0 from tensile properties, compared using experiments, the error of FLC_0 calculated with the proposed model is within 10%. In the IB model, the left side of FLC can be calculated using a line with a slope of -1 while the right side of the FLC is obtained via a modified Keeler model with the exponent (p) determined as 0.45 for hot-rolled steels. Complete experimental FLCs of hot-rolled steels from measurements and the literature were used to validate the reliability of the proposed model. Resultantly, the prediction of FLCs with the proposed IB model is greatly improved, and agrees much better with the experimental FLCs than the predictions of the well-known Keeler model, Arcelor model and Tata Steel model.

Keywords: forming limit curve (FLC); phenomenological model; IMR-Baosteel model; tensile property; hot-rolled steel

check for updates

Citation: Chen, W.-J.; Song, H.-W.; Chen, S.-F.; Xu, Y.; Deng, S.-Y.; Cai, Z.; Pei, X.-H.; Zhang, S.-H. A New Phenomenological Model to Predict Forming Limit Curves from Tensile Properties for Hot-Rolled Steel Sheets. *Metals* **2024**, *14*, 168. https://doi.org/10.3390/met14020168

Academic Editor: Mohammad Jahazi

Received: 2 December 2023
Revised: 2 January 2024
Accepted: 10 January 2024
Published: 29 January 2024

1. Introduction

Hot-rolled high-strength steels are employed widely in chassis parts of passenger cars and commercial vehicles to reduce automotive weight for energy saving and carbon dioxide emission reduction [1–3]. In the automotive industry, excessive thinning or necking are both unacceptable. When sheet thickness is reduced and material strength increases, the formability of the material is always decreased. It is an especially great challenge to produce complex components with high-strength steels, which always need trial and error iterations for the design of the component profile and the forming process [4]. Thus, accurate evaluation of hot-rolled sheet formability is essential for improving design efficiency and the quality of complex components.

The concept of the forming limit curve (FLC) was initially proposed in 1963 [5], and was usually determined from standard experiments using the Marciniak [6] test or the Nakazima test [7]. Nowadays, the FLC is popularly chosen to provide efficient prediction of the failure risk in sheet metal forming processes [8–10]. In the FLC, the FLC_0 is the forming limit under plane strain conditions, which is near the vertical axis and is usually the lowest point of the FLC. The strain values of the FLC are usually determined through strain measurement procedures on gridded specimens. The main problem is that the experimental determination of the FLC is always costly, time-consuming and inconsistent, and the measurement results highly depend on the mechanical properties of the specimen being tested at that time. Another problem is that friction affects the location, deformation behavior and strain path of the necking point during the experimental tests [11]. In order to improve the quality and efficiency of FLC experiments, many test methods have been developed. A new procedure based on the hydraulic bulging of a double specimen was proposed for the experimental determination of the FLCs to reduce the frictional effects [12]. A test procedure for determining the complete left-hand side of the FLC via tensile tests without friction was outlined [13]. A method was developed to determine the width of specimens to obtain the FLC with the minimum number of tests [14]. However, shortcomings in FLC testing such as laborious measurement and data discretization still cannot be overcome.

Then, much work has been performed to determine the FLC more cheaply, efficiently and accurately during the last few years. One research direction is to develop theoretical models to estimate the FLC. The Hill–Swift model is based on the Swift diffuse instability theory [15] and the Hill localized instability theory [16], and has been expanded to many modified models. However, it has been reported that the Hill–Swift model delivers too-small FLD_0 values [17]. The Marciniak–Kuczyński (MK) model is the most widely used model to estimate the necking limit strain for sheet metals [18]. However, it is not popular to estimate the formability of hot-rolled steels with the MK model. This is because the characteristics of hot-rolled steels are weak anisotropy and a low strain hardening exponent, which are different from cold-rolled steel, stainless steel and aluminum alloy [19,20]. Furthermore, it is typical to calculate the forming limit under plane stress conditions with these theoretical models, and the relationship between the through-thickness stress and sheet thickness was ignored. The nonconstant through-thickness normal stress was presented as a critical factor in the FLC prediction for medium plate [21]. For hot-rolled steels with a larger thickness range, the complicated calculation process of the FLC cannot meet the need for efficient formability evaluation in the automotive industry [22].

Another research direction is to develop empirical methods from simple and low-cost experiments to predict the FLC. Empirical methods based upon basic mechanical properties through tensile tests to predict the FLC have been popular for many decades [23]. Keeler and Brazier [24] proposed a regression equation to predict the FLC_0 with a strain hardening exponent and thickness. Raghavan [25] described an equation to predict the FLC_0 with total elongation and sheet thickness. Paul [26,27] proposed a nonlinear regression equation to predict the FLC_0 with ultimate tensile strength, total elongation, strain hardening exponent and sheet thickness. Cayssials [28] developed a predictive method with the strain rate sensitivity, the strain hardening and the sheet thickness based on plastic instability and damage theories. Furthermore, the model was extended by Cayssials [29] to predict the FLC of ultrahigh-strength steels with ultimate tensile strength, uniform elongation, the anisotropy coefficient and the sheet thickness; this is called the Arcelor model. Abspoel [30,31] developed a model to predict the FLC with four strain points including the uniaxial tensile necking point, the plane strain point, the intermediate biaxial stretching point and the equi-biaxial stretching point. The four representative points are calculated using the Lankford coefficient, total elongation and sheet thickness. This model is also called the Tata Steel model. Gerlach [32,33] provided equations to calculate the three characteristic points of the FLC based on three parameters, including ultimate tensile strength, total elongation and sheet thickness. Among these empirical methods, the Keeler model, Arcelor model and Tata Steel model have been integrated into commercial finite element simulation software AutoForm R5.2 [34]. However, since these predictive models are mainly developed from cold-rolling steel sheets or aluminum alloy sheets, the FLC prediction results for hot-rolled steel sheets have a large deviation from the experimental results.

Consequently, in order to shorten the time for the forming process design and reduce the test costs, a reliable phenomenological model named the IMR-Baosteel model (IB model) is established based upon tensile properties in this work, and can effectively predict the formability of hot-rolled steel sheets.

2. Prediction of FLD_0 with Classic Empirical Models for Hot-Rolled Steel Sheets

2.1. Data Collection from Experimental Tests

The tensile test is the most widely used method to determine the mechanical properties of materials. Therefore, empirical models are always derived from the statistical relations between the experimental FLC points and the mechanical properties. The details of the test data measured from the Baosteel laboratory are tabulated in Appendix A (Table A1). There are almost eighty hot-rolled steel sheets in various thickness and strength ranges for this investigation obtained from regular steel production in the Baosteel workshop. Figure 1a shows the range of the mechanical properties. The ultimate tensile strength varies between 200 MPa and 1100 MPa, and the total elongation varies between 10% and 50%. The thickness of the sheets varies between 1.5 mm and 6.0 mm, as shown in Figure 1b.

The mechanical properties were obtained from uniaxial tensile tests, performed according to ISO 6892-1:2019 [35], on Instron testing equipment. The collected mechanical properties are yield strength R_p, ultimate tensile strength R_m, total elongation A_t, uniform elongation A_g, the plastic strain ratio r-value and strain hardening exponent n-value. The r-values and the n-values were determined between 2% and 20% strain or between 2% and Ag when the A_g was lower than 20%, according to ISO 10113:2020 [36] and ISO 10275:2020 [37], respectively. The gauge length L_0 to measure A_t is correlated with sheet thickness, which can be determined as

$$L_0 = 5.65 * \sqrt{t * b_0} \tag{1}$$

where b_0 is the specimen width of the measurement area in the tensile test.

The experimental strains of FLC_0 and complete FLCs were obtained from Nakazima tests according to ISO 12004-2: 2008 [38] using a 750 KN Interlaken sheet metal testing machine with the Vialux photogrammetric measurement system. A pattern of 2 mm square grids was applied to the surface of the specimens using the electrochemical method. Then the specimens were deformed until fracture using a hemispherical punch with a diameter of 100 mm. Ten specimens with the same length of 196 mm but different widths (varying from 20 mm to 180 mm) were selected to obtain limit strains under different loading paths. Finally, the complete experimental FLCs were obtained with these limit strains under different strain states. The specimens were measured transverse to the rolling direction. Additionally, two specimens of the same size were tested to take the average value. The FLC_0 is usually determined using the widths of 90 mm and 100 mm, which are nearest to the plane strain state.

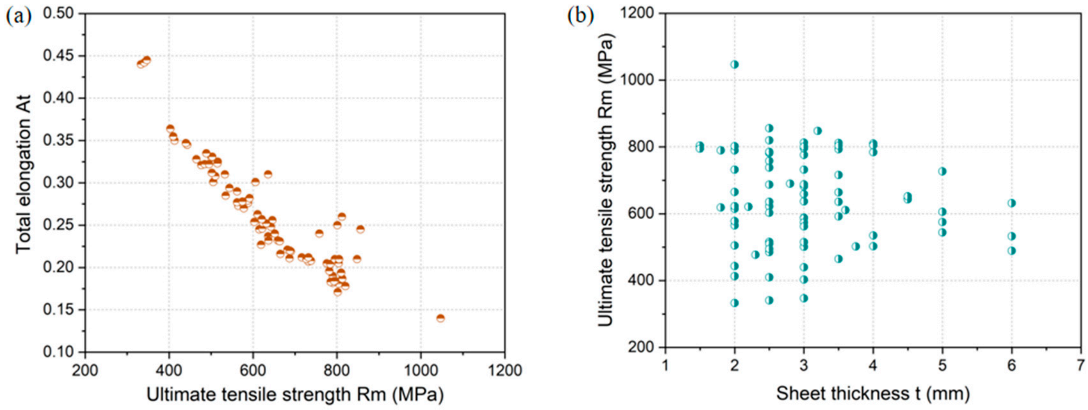

Figure 1. Mechanical properties of eighty measured hot-rolled steels: (**a**) total elongation with ultimate tensile strength, and (**b**) ultimate tensile strength with sheet thickness.

FLC_0 is the forming limit for plane strain conditions, and denotes the lowest point of the FLC. So the accurate determination of the FLC_0 is primarily important for predicting the FLC. Experimental FLC_0 values were plotted with mechanical properties, and the influence of these mechanical properties on the characteristics of the FLC_0 was studied.

Figure 2 shows the correlation between the FLC_0 and tensile properties. R_p (Figure 2a), R_m (Figure 2b), A_g (Figure 2c), A_t (Figure 2d) and the n-value (Figure 2e) show an approximately linear trend with the FLC_0, while there is no significant correlation between the FLC_0 and the r-value (Figure 2f) or thickness t (Figure 2g). Furthermore, among these mechanical properties obtained from regular tensile tests, the coefficients of determination of three properties including A_g, A_t and the n-value are more than 0.8, which shows a stronger correlation with the FLC_0.

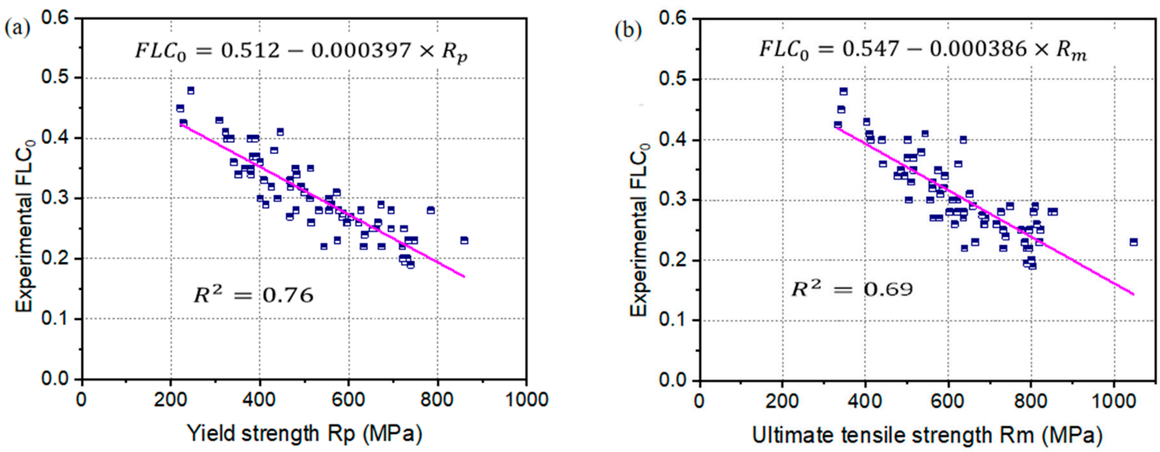

Figure 2. *Cont.*

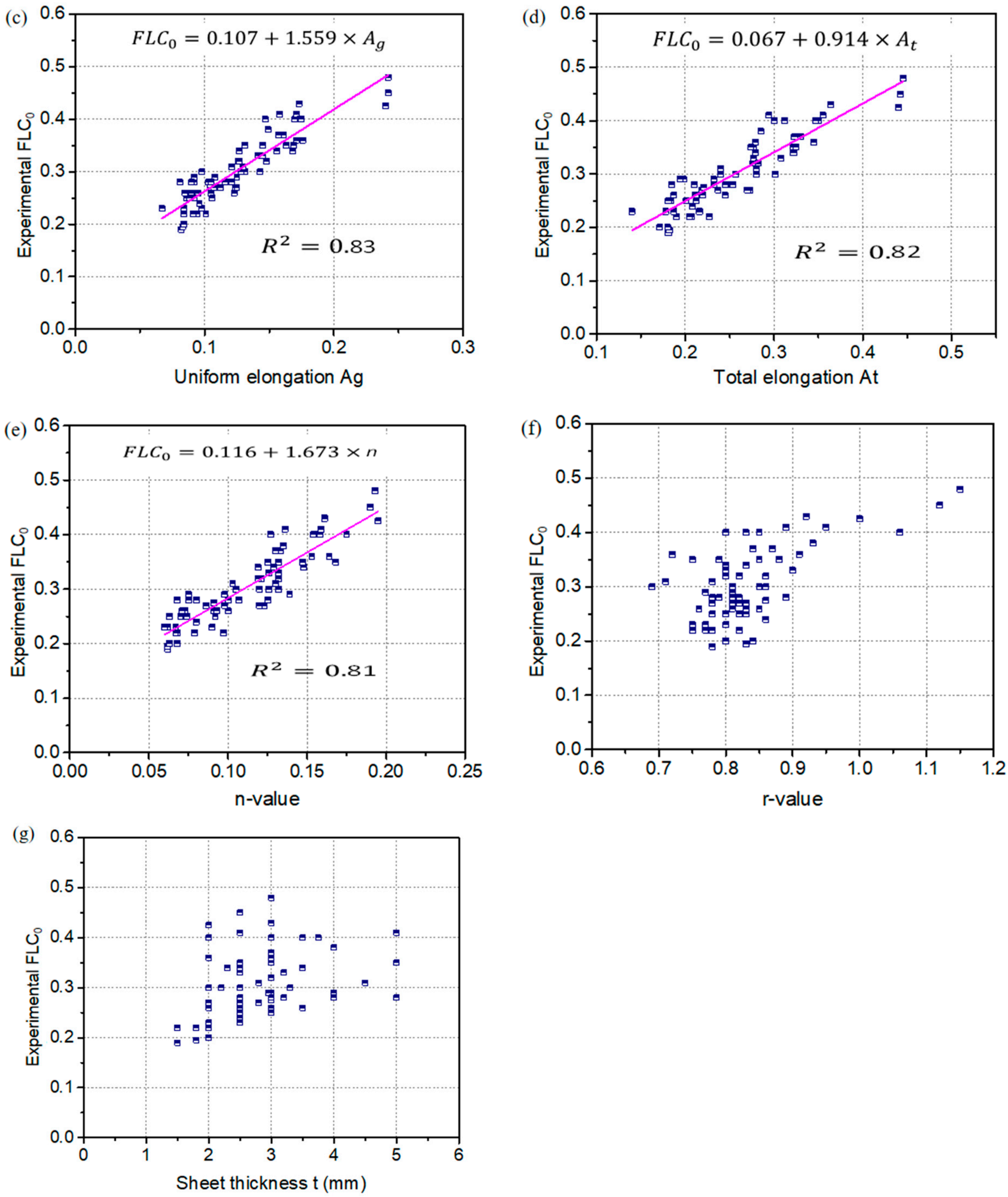

Figure 2. Correlation between FLC_0 and tensile properties: (**a**) yield strength (R_p), (**b**) ultimate tensile strength (R_m), (**c**) uniform elongation (A_g), (**d**) total elongation (A_t), (**e**) strain hardening exponent (n-value), (**f**) plastic strain ratio (r-value) and (**g**) sheet thickness (t).

2.2. Prediction Results for FLC_0 with Classic Empirical Models

The Keeler model is the most popular method for predicting the FLC, especially in the automotive industry [39]. However, the comparison showed that the Keeler model was only reliable for classic forming-grade steels [40]. In this section, these classic empirical models including the Keeler model, Raghavan model, Paul model, Tata Steel model and Arcelor model are employed to verify the prediction reliability for hot-rolled steel sheets.

The collected FLC_0 data of hot-rolled steel sheets are grouped according to sheet thickness and tensile strength.

The Keeler model is shown as

$$FLC_0 = ln\left[1 + \left(\frac{23.3 + 14.13 * t}{21}\right) * n\right] \quad (2)$$

The Raghavan model is shown as

$$FLC_0 = 2.78 + 3.24 * t + 0.892 * A_t \quad (3)$$

The Paul model is expressed as

$$FLC_0 = 7.702 * exp(-0.0122 * R_m) - 0.1124 * r - 0.6908 * exp(-12.4187 * A_t) + 0.1149 * n + 0.0823 * t + 0.3011 \quad (4)$$

The Tata Steel model is expressed as

$$FLC_0 = 0.0084 * A_t + 0.0017 * A_t * (t - 1) \quad (5)$$

Furthermore, the equation for the Arcelor model was not provided in papers and the FLC prediction can be obtained from AutoForm R7 [41].

First, the calculation results from the well-known empirical models were compared with the experimental FLC_0 according to the stratification of sheet thicknesses. For sheets of a thickness less than 3 mm, as shown in Figure 3a, the Keeler model and Arcelor model can predict well for sheets with high formability, and the predicted deviation is even lower than 10%. However, the Keeler model and Arcelor model severely underestimate the FLC_0 of sheets with low formability. The Paul model and Raghavan model slightly overestimate the FLC_0, with the predicted deviation between 10% and 30%, while the Tata Steel model underestimates the formability, with the deviation exceeding 10%. For sheets of a thickness greater than 3 mm, as shown in Figure 3b, the prediction results with the above models have a large scatter. The predicted deviations of the Keeler model, Raghavan model and Tata Steel model are barely less than 30%.

Second, the calculation results using the well-known empirical models were compared with the experimental FLC_0 according to the stratification of tensile strength. For the sheets with a tensile strength lower than 550 MPa, as shown in Figure 3c, the Paul model and Raghavan model slightly overestimate the FLC_0 while the Tata Steel model slightly underestimates the FLC_0 with the predicted deviation almost between 10% and 30%. In comparison, the Keeler model has the best prediction accuracy with a deviation less than 10%. For the sheets with a tensile strength higher than 550 MPa, as shown in Figure 3d, the prediction accuracy of these empirical models is much more unreliable. The predicted deviation of the Raghavan model is just near 30%, while the predicted deviation of the other models actually even exceeds 30%.

In summary, for hot-rolled steel sheets, when the sheet thickness is less than 3.0 mm and tensile strength is lower than 550 MPa, the prediction accuracy of the Keeler model is comparatively reliable. However, when the sheet thickness is greater than 3.0 mm or the tensile strength is greater than 550 MPa, the prediction accuracy of the above five empirical models is significantly poor.

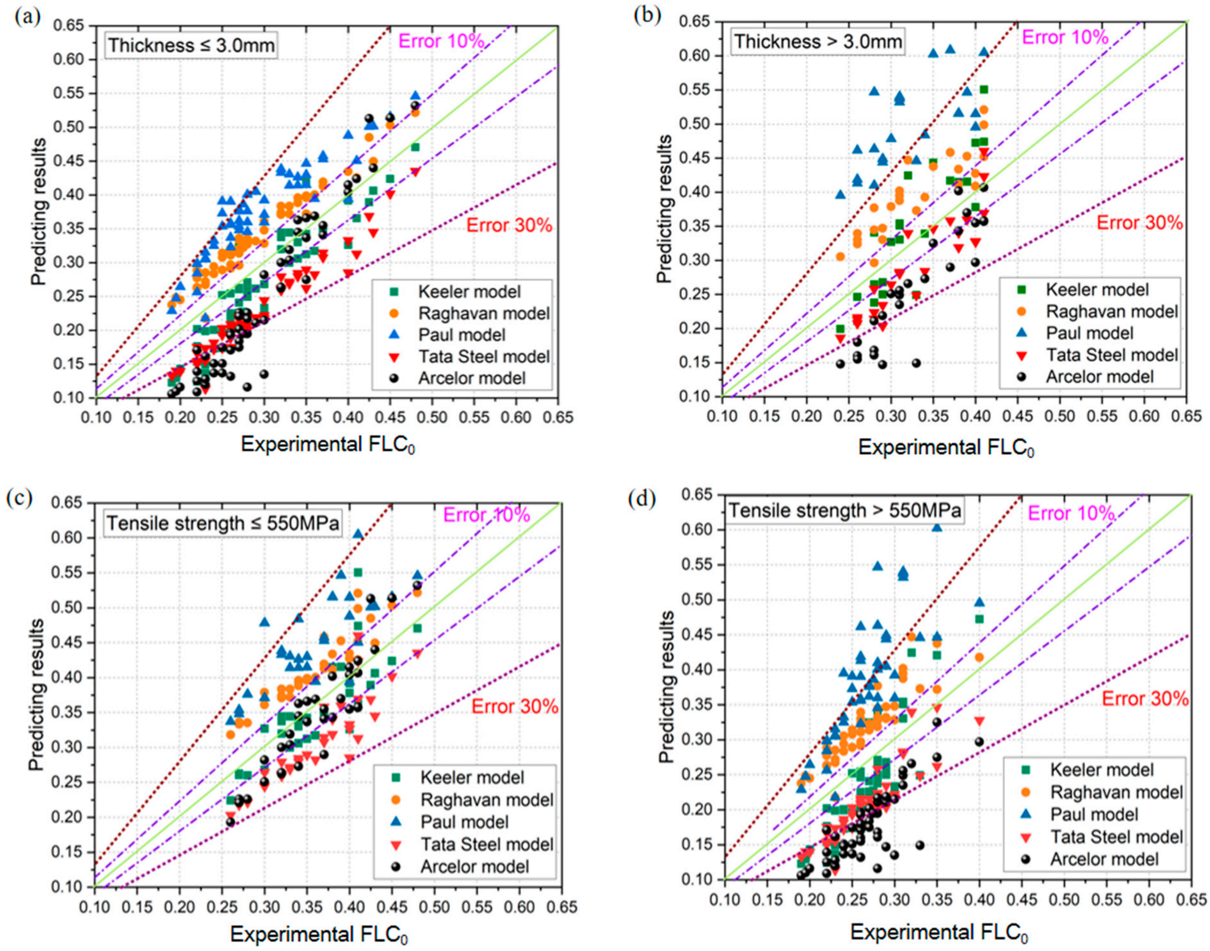

Figure 3. Prediction of plane strain forming limit (FLC$_0$) of hot-rolled steel sheets by different empirical models under the following conditions: (**a**) sheet thickness less than 3 mm, (**b**) sheet thickness greater than 3 mm, (**c**) sheet tensile strength lower than 550 MPa and (**d**) sheet tensile strength higher than 550 MPa.

2.3. Critical Mechanical Properties for FLD$_0$ Prediction

In a standard uniaxial tensile test, the digital image correlation (DIC) method is used to measure strain and elongation. Figure 4a shows the engineering stress–strain curve of hot-rolled high-strength steel S550MC with a thickness of 2.5 mm. The engineering stress–strain curve is transformed into the real stress–strain curve by fitting the index; then, the n-value can be obtained. The n-value is often used to describe sheet formability as an important parameter, such as in the Keeler model. However, as shown in Figure 4b, there is a yield plateau on the engineering stress–strain curve of hot-rolled steel. Due to that, it is not sufficient to describe the stress–strain behavior with the power law equation [42], which further means the n-value obtained from the power law equation cannot accurately capture the actual strain hardening behavior.

Figure 4c shows the true plastic strain measurement of the local necking point in the uniaxial tensile test. It can be seen that the plastic strain in the whole narrow region of the test specimen is uniform before the time of the maximum uniaxial tensile force. During this period, the strain ratio of the true plastic width strain to the true plastic longitudinal strain is stable at $-1/2$. It is worth mentioning that, at the time of maximum uniaxial tensile force, the uniform elongation is approximately equal to the true plastic longitudinal strain. After the time of maximum uniaxial tensile force, the region where the plastic strain increment continues reduces gradually until local instability and fracture occur. Simultaneously, the strain state changes from uniaxial tension to a plane strain condition. It is clear that the distance between the uniform elongation point and local onset necking point is long for hot-rolled steel sheets. The local onset necking point is much closer to the specimen fracture point which corresponds to the total elongation. Therefore, a stronger correlation between A_t and the FLC_0 rather than Ag is verified.

Furthermore, the effect of sheet thickness on the FLC_0 has been widely reported in the literature [43,44]. And the influence of thickness on the FLC is significant especially for hot-rolled steel sheets; the explanation for this is that as thickness increases, local necking becomes more diffuse and the time to reach the critical depth of fracture which is defined as failure is increased [45].

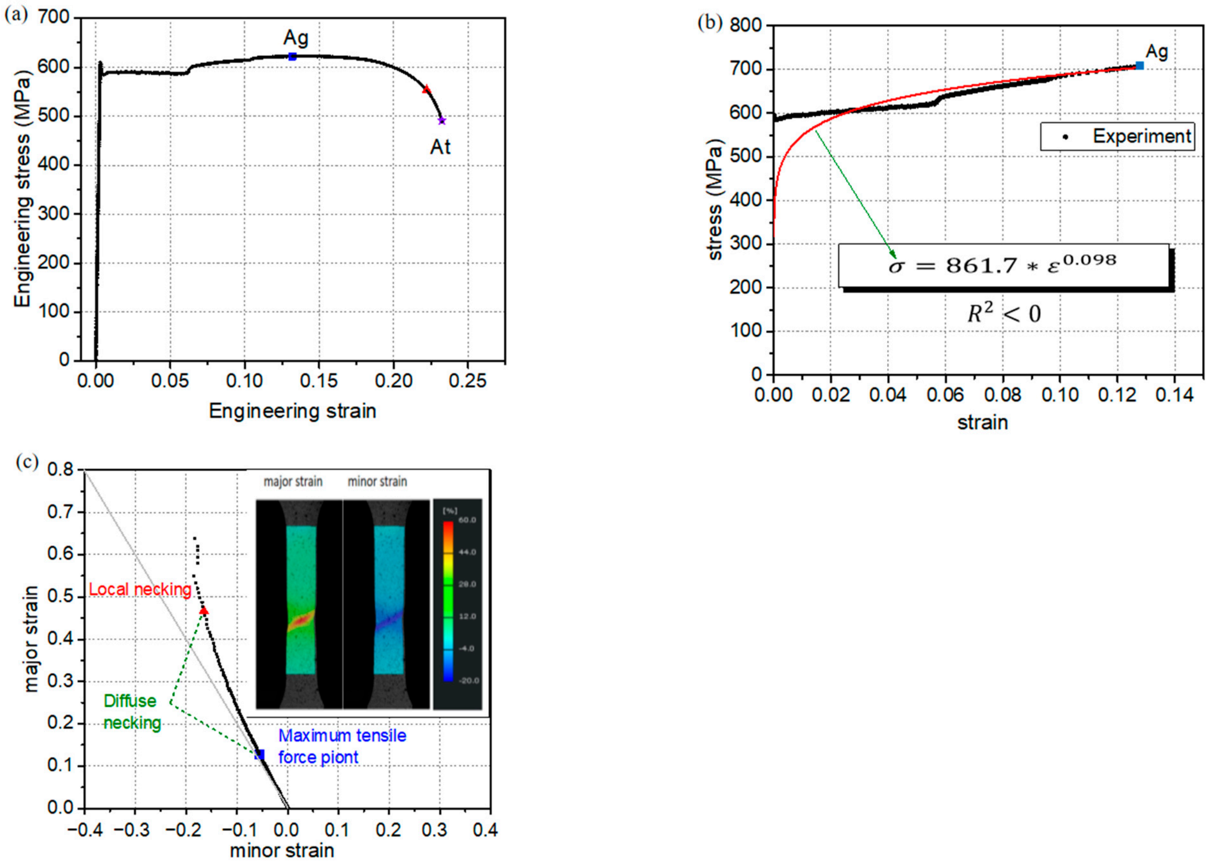

Figure 4. Measurement during uniaxial tensile test for S550MC: (**a**) engineering stress–strain curve, (**b**) true stress–strain curve and fitting and (**c**) strain path tracking at local necking point using DIC.

3. Establishment of New Prediction Model for FLC_0

According to the above analysis, the key parameters of A_t and thickness t were adopted to establish the prediction model of the FLC_0 in this work. The experimental data of FLC_0 with different thicknesses of hot-rolled steel sheets were extracted to investigate the mathematical relation between the FLC_0 and the total elongation A_t, along with the thickness.

As illustrated in Figure 5, the correlation of A_t with the FLC_0 was studied from the typical thicknesses 2.0 mm, 2.5 mm and 3.0 mm. It is obvious that the correlation of the FLC_0 with A_t is not linear at different thicknesses. Then, a cubic polynomial equation was used to regress the correlation of FLC_0 with A_t:

$$FLC_0 = A_0 + A_1 * A_t + A_2 * A_t^2 + A_3 * A_t^3 \quad (6)$$

$A_0 A_1 A_2 A_3$ are the constant parameters of the cubic polynomial equation. Then the parameters were fitted from the data in Figure 5a–c, and are summarized in Table 1.

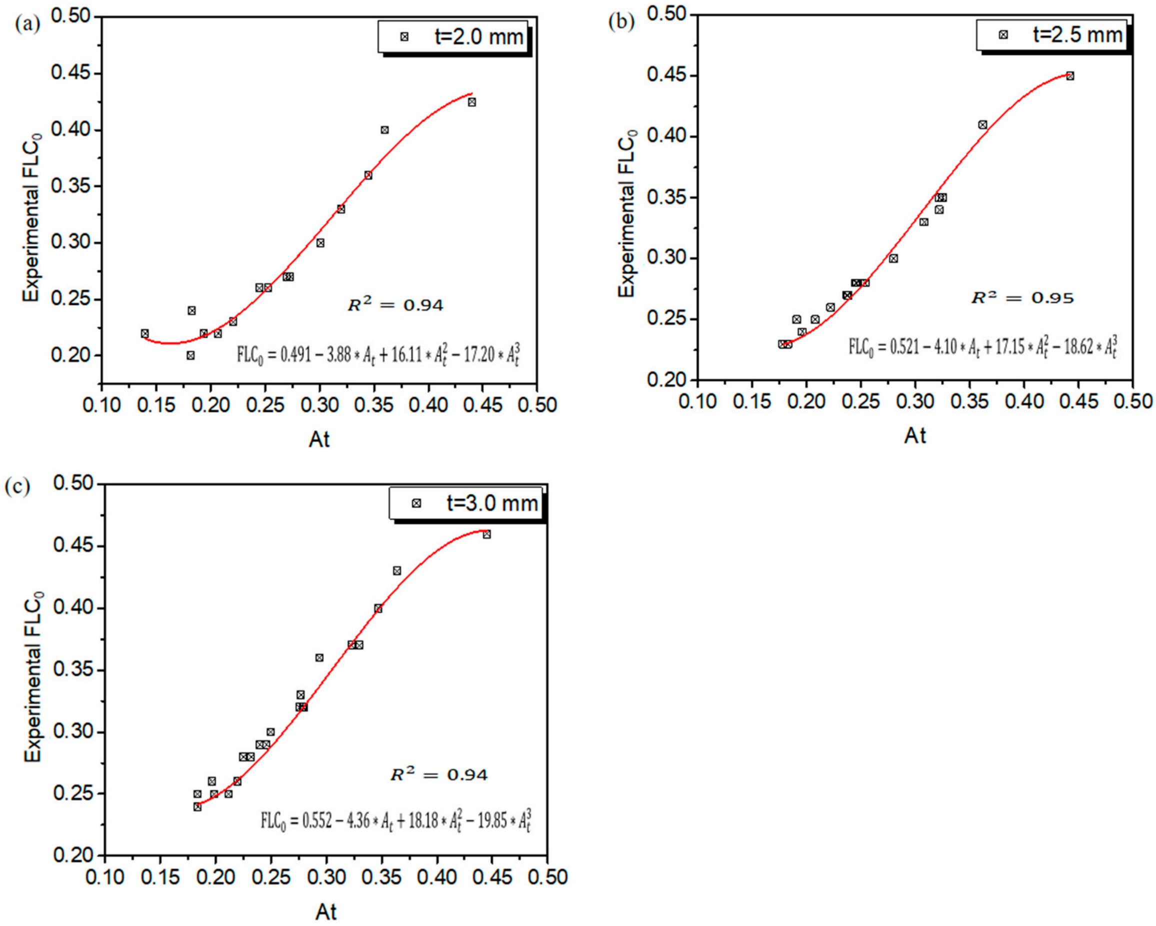

Figure 5. Regression of FLC_0 with total elongation: (**a**) sheet thickness 2.0 mm, (**b**) sheet thickness 2.5 mm and (**c**) sheet thickness 3.0 mm.

Table 1. The fitting parameters of the cubic polynomial equation.

t (mm)	A_0	A_1	A_2	A_3
2.0	0.491	−3.88	16.11	−17.20
2.5	0.521	−4.10	17.15	−18.62
3.0	0.552	−4.36	18.18	−19.15

Furthermore, the influence of thickness on the FLC_0 was studied based on the FLC_0 of 2.0 mm thickness. The correlation ratio between strain and thickness (CRST) is defined as the ratio of the FLC_0 of other thicknesses to the FLC_0 of 2.0 mm. The individual experimental FLC_0 of QStE600 TM at different thicknesses, including 2.0 mm, 2.5 mm, 3.5 mm and 5.0 mm, was employed to determine the CRST. The calculating results for the CRST are shown in Table 2.

Table 2. The determination of CRST for QStE600TM.

t (mm)	FLC_0	CRST
2.0	0.22	1
2.5	0.24	1.091
3.5	0.26	1.182
5.0	0.28	1.273

Then the CRST data were plotted vs. the thickness, as shown in Figure 6. The CRST can be calculated as

$$CRST = 1.05 * (t - 1.31)^{0.142} \tag{7}$$

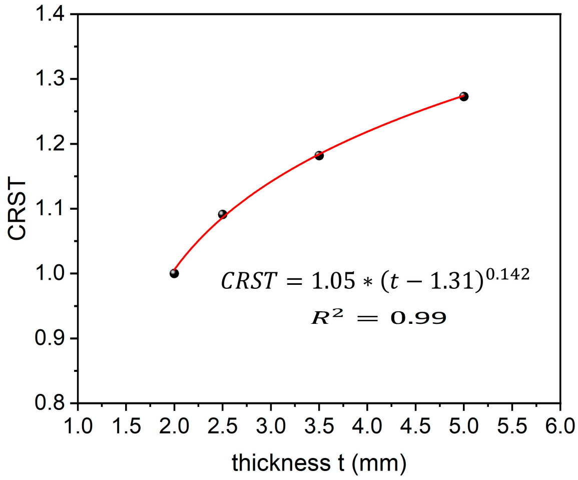

Figure 6. Correlation ratio with strain and thickness (CRST) vs. thickness.

Combining Equations (6) and (7), the predictive model of the FLC_0 with total elongation and thickness is established as

$$FLC_0 = \left(0.491 - 3.88 * A_t + 16.11 * A_t^2 - 17.20 * A_t^3\right) * 1.05 * (t - 1.31)^{0.142} \tag{8}$$

Figure 7 shows the prediction capability of the proposed model compared with the Keeler model. It is clear that the predicted deviations calculated with the Keeler model mostly exceed 10% and even exceed 30% for high-strength steel sheets. By contrast, the predicted deviations calculated with the proposed model are almost under 10%. The results show that the proposed model can accurately predict the FLC_0 for hot-rolled steel sheets and the performance is much better than that of the Keeler model in the area of high-strength steel sheets especially.

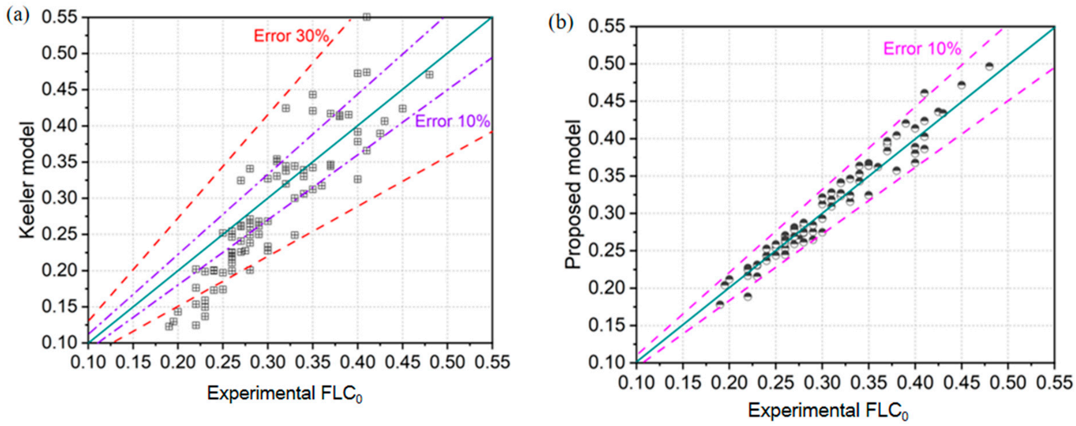

Figure 7. Prediction of plane strain forming limit (FLC_0) of various steel sheets with (**a**) Keeler model and (**b**) the proposed model.

4. Determination of Phenomenological Model for Complete FLC

A complete FLC consists of two limit curves located in the tension–tension and tension–compression domains, respectively. The FLC covers almost the entire deformation domain in the sheet metal forming processes. In general, the strain ratio spans between those induced by uniaxial and equi-biaxial loads.

Levy [46] described that the slope of the uniaxial tensile strain path in the forming limit diagram depends upon the r-value. The higher the r-value, the greater the slope of the uniaxial tensile strain path in the forming limit diagram. However, hot-rolled steels have the characteristic of weak anisotropy. The distribution of r-values for hot-rolled high-strength steel is concentrated between 0.7 and 0.9 (Figure 2f). As a result, the shapes of FLC curves for hot-rolled steel sheets are almost similar and the main difference is the height of the curves.

According to [24], the left side of the strain-based FLC can be calculated with an equation with a slope of −1:

$$\varepsilon_1 = FLC_0 - \varepsilon_2 \tag{9}$$

where ε_1 is major strain and ε_2 is minor strain.

Then the right side of the strain-based FLC can be calculated with [26]:

$$\varepsilon_1 = (1 + FLC_0)(1 + \varepsilon_2)^p - 1 \tag{10}$$

where p is a material constant.

To determine the parameter of p, the experimental FLCs of SAPH440, QStE460TM, QStE600TM and S700MC were employed for further analysis.

FLC_0 can be calculated with Equation (8), the left side of the FLC can be calculated with Equation (9) and the right side of the FLC can be calculated with Equation (10) with different values of p, as shown in Figure 8. The right side of the predicted FLC agrees well with the experimental FLC. Therefore, p was determined as 0.45 for hot-rolled steels. Furthermore, the left side of the FLC predicted with Equation (9) also agrees well with the experimental FLC.

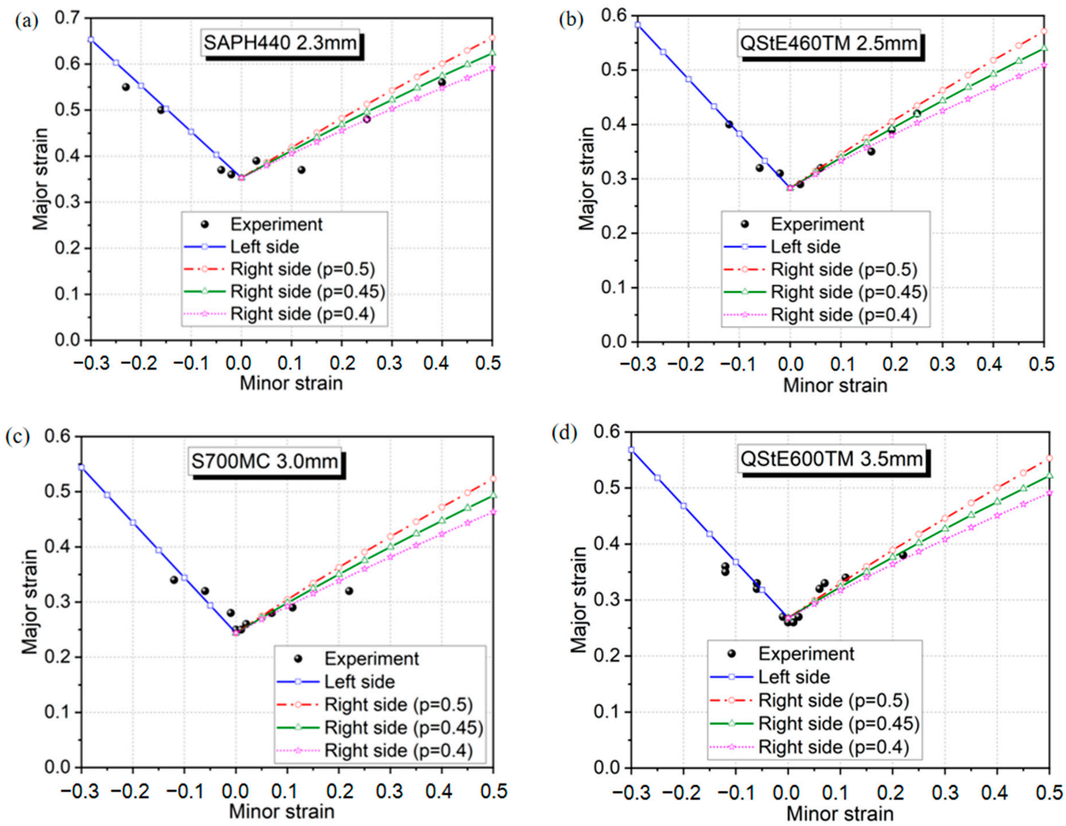

Figure 8. The determination of p from experimental FLCs: (**a**) SAPH440 2.3 mm, (**b**) QStE460TM 2.5 mm, (**c**) QStE600TM 3.5 mm and (**d**) S700MC 3.0 mm.

Therefore, the new phenomenological model for the complete FLC of hot-rolled steel sheets can be determined with the combination of Equations (8)–(10). This phenomenological model is named the IMR-Baosteel model, which is shortened to the IB model. Then several experimental FLCs were collected to validate the reliability of the IB model compared with well-known models including the Keeler model, Arcelor model and Tata Steel model.

On one hand, the experimental FLCs of SAPH440, S550MC, S700MC and FB780 tested in the laboratory were employed to verify the reliability of the IB model. As illustrated in Figure 9a, the experimental FLC of low-strength steel SAPH440 can be predicted well with both the Keeler model and the proposed IB model. The left-hand side of the Tata Steel model and the right-hand side of the Arcelor model agree with the experimental points. In contrast, the slopes of the right-hand side of the Tata Steel model and the left-hand side of the Arcelor model deviate from the experimental points. Then the prediction of FLCs with the proposed IB model can agree with the experimental FLCs for hot-rolled high-strength steels (Figure 9b–d). However, these three classic empirical models cannot accurately predict the FLC, and the main deviation derives from the underestimated prediction of the FLC_0, especially for high-strength steels.

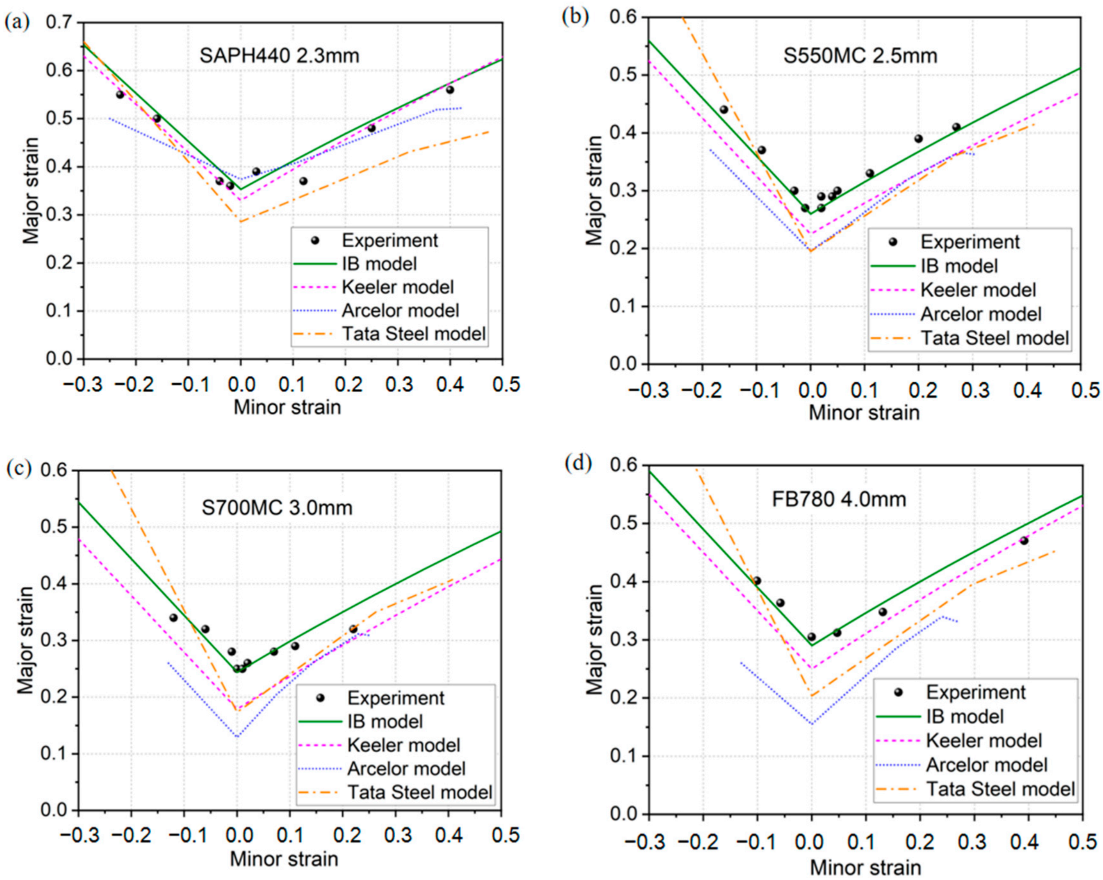

Figure 9. Prediction of complete forming limit diagram with proposed model for various steel sheets: (**a**) SAPH440, (**b**) S550MC, (**c**) S700MC and (**d**) FB780. Experimental FLCs are collected from measurement.

On the other hand, the experimental FLCs of the SAPH370, QStE340TM, QStE550TM, 580DP, 700DP and Q-P-T steels were collected from the literature to verify the reliability of the IB model. As shown in Figure 10a–c, for SAPH370, QStE340TM and QStE550TM steel, it is clear that the Keeler model slightly underestimates the height of the FLC, while it overestimates the height of the FLC for 580DP and 700DP steel (Figure 10d,e). The Arcelor model and Tata Steel model both underestimate all of these FLCs except SAPH370. Generally, the curve slope of the left-hand side predicted with the Tata Steel model overestimates the measuring points while the curve slope of the right-hand side predicted with the Tata Steel model underestimates the measuring points. Obviously, the prediction with the IB model agrees better with the experimental FLCs (Figure 10a–e). For quenching–partitioning–tempering (Q-P-T) steel (Figure 10f), the IB model can predict the FLC_0 well. However, the IB model overestimates the left side of the FLC and underestimates the right side of the FLC, perhaps due to the low r-value, about 0.27, of Q-P-T steel.

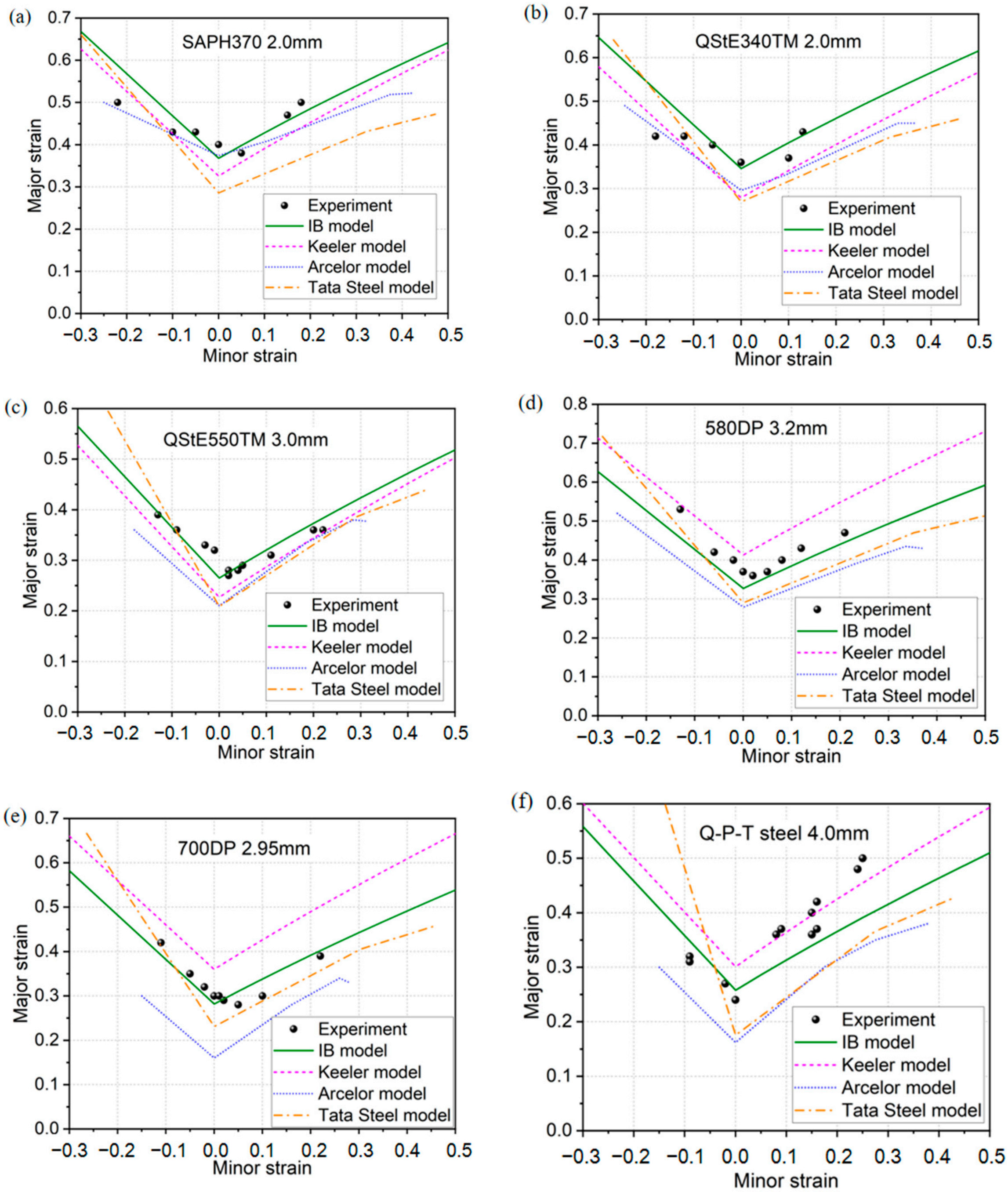

Figure 10. Prediction of complete forming limit diagram by various models for various steel sheets: (**a**) SAPH370, (**b**) QStE340TM, (**c**) QStE550TM, (**d**) 580DP, (**e**) 700DP and (**f**) Q-P-T steel. Experimental FLCs data were adapted from Refs. [20,21,47].

5. Conclusions

In this work, a new phenomenological model named the IB model based on tensile properties is proposed to predict the FLC for hot-rolled steel sheets accurately and efficiently. The main conclusions can be summarized as follows:

(1) The effect of tensile properties on the plane strain forming limit (FLC_0) was studied with experimental results of eighty hot-rolled steel sheets under various thicknesses and strengths. Classic empirical models were employed to verify the prediction reliability. The results show that when the sheet thickness is less than 3.0 mm and the tensile strength is lower than 550 MPa, the Keeler model has the best prediction accuracy, with a deviation of less than 10%, which is better than other empirical models. However, there are distinct deviations in predicting hot-rolled high-strength steel sheets with all of the current empirical models. For high-strength hot-rolled steel sheets, the Keeler model almost underestimates the FLC, due to the fact that hot-rolled steels have the characteristics of a low strain hardening exponent and higher thickness.

(2) For hot-rolled steels, there is a yield plateau on the engineering stress–strain curve. Due to this, it is not sufficient to describe the stress–strain behavior with the power law equation, which means the n-value obtained from power law equation fitting cannot describe the hardening behavior accurately. Combined with the correlation analysis and DIC measurement during the tensile test, it was found that there is a stronger regression relationship between the total elongation and the FLC_0. Then the IB model, combining the cubic polynomial equation and power equation, was proposed to regress the correlation of the FLC_0 with total elongation and thickness. The errors calculated for the FLC_0 with the proposed model are mainly under 10% compared with the errors calculated with the Keeler model, which exceed 30–50% for hot-rolled high-strength steels. Additionally, the IB model is applicable for thicknesses between 1.5 mm and 6.0 mm, which covers most hot-rolled steels being employed. And its reliability for hot-rolled steels out of this thickness range is not verified with effective experimental data.

(3) In the IB model, the left side of the FLC can be calculated via a line with a slope of −1 for the majority of hot-rolled steels with r-values between 0.7 and 0.9, while the right side of the FLC can be obtained via a modified Keeler model with the exponent (p) determined as 0.45 for hot-rolled steels. Ten complete experimental FLCs of hot-rolled steels from measurements and the literature were used to validate the prediction reliability. The results show that the prediction of the complete FLC with the IB model matches much better with the experimental FLC than those with the other empirical models. However, for Q-P-T steel, the IB model can predict the FLC_0 well but cannot predict the left and right sides of the FLC accurately, due to the low r-value of about 0.27.

Author Contributions: Conceptualization, H.-W.S., X.-H.P. and S.-H.Z.; methodology, W.-J.C., H.-W.S. and S.-Y.D.; investigation, W.-J.C. and Z.C.; writing—original draft preparation, W.-J.C. and S.-Y.D.; writing—review and editing, H.-W.S., S.-F.C., X.-H.P., Z.C. and Y.X.; supervision, S.-H.Z.; funding acquisition, S.-F.C. and Y.X. All authors have read and agreed to the published version of the manuscript.

Funding: This research was funded by the National Key Research and Development Program of China (grant number 2022YFB3304800), the National Natural Science Foundation of China (grant number 52111530293 and grant number 52105412), the project of the Institute of Metal Research, Chinese Academy of Sciences (grant number E055A501) and the scientific and technological cooperation project between Jilin Province and the Chinese Academy of Sciences (grant number 2022SYHZ0007).

Data Availability Statement: All data are contained within the article and in the Refs. [20,21,47].

Acknowledgments: The authors would like to thank Qin-Bo Shen and Hua Zhang from Baosteel Research Institute for their help with the experimental phase of this work.

Conflicts of Interest: Authors Zheng Cai and Xin-Hua Pei were employed by the company Research Institute, Baoshan Iron and Steel Co., Ltd. The remaining authors declare that the re-search was conducted in the absence of any commercial or financial relationships that could be construed as a potential conflict of interest.

Appendix A

Table A1. Uniaxial tensile properties and experimental FLC_0 for data analysis.

Steel	t (mm)	Rp (MPa)	Rm (MPa)	n-Value	r-Value	Ag	At	Exp FLC_0	Cal FLC_0	Keeler FLC_0
SPHC	2	228	333	0.195	1	0.24	0.44	0.425	0.436	0.389
SPHC	2.5	222	341	0.19	1.12	0.242	0.442	0.45	0.472	0.424
SPHC	3	245	347	0.193	1.15	0.242	0.445	0.48	0.496	0.471
SAPH370	2	326	413	0.158	1.06	0.17	0.35	0.4	0.368	0.326
SAPH370	2.5	323	410	0.157	0.95	0.171	0.355	0.41	0.403	0.366
SAPH370	3	309	403	0.161	0.92	0.173	0.364	0.43	0.434	0.406
SAPH400	2	341	443	0.153	0.91	0.171	0.345	0.36	0.362	0.317
SAPH400	3	335	440	0.154	0.83	0.174	0.347	0.4	0.414	0.392
SAPH440	2.3	352	477	0.148	0.8	0.168	0.321	0.34	0.353	0.330
SAPH440	2.5	366	485	0.147	0.79	0.169	0.322	0.35	0.364	0.342
SAPH440	3.5	343	465	0.149	0.83	0.171	0.328	0.38	0.404	0.415
SPFH540	2	467	565	0.123	0.78	0.124	0.273	0.27	0.281	0.263
SPFH540	3	493	588	0.121	0.8	0.126	0.276	0.32	0.323	0.320
SPFH590	2	515	615	0.1	0.81	0.09	0.245	0.26	0.253	0.218
SPFH590	2.5	532	622	0.102	0.86	0.094	0.246	0.28	0.275	0.249
SPFH590	4.5	542	646	0.095	0.76	0.099	0.256	0.31	0.328	0.331
QStE340TM	2.5	379	516	0.132	0.85	0.163	0.325	0.35	0.367	0.312
QStE340TM	3	383	501	0.130	0.87	0.161	0.33	0.37	0.392	0.347
QStE380TM	2	401	505	0.126	0.81	0.143	0.301	0.3	0.312	0.268
QStE380TM	2.5	409	510	0.126	0.8	0.141	0.308	0.33	0.346	0.300
QStE380TM	3.75	378	502	0.127	0.85	0.147	0.312	0.4	0.389	0.378
S355MC	2.5	380	495	0.129	0.77	0.156	0.322	0.34	0.364	0.306
S355MC	3	392	515	0.132	0.87	0.157	0.323	0.37	0.383	0.344
S355MC	4	369	503	0.136	0.81	0.159	0.331	0.39	0.421	0.415
S355MC	6	378	489	0.143	0.86	0.168	0.335	0.41	0.461	0.550
S420MC	2	467	578	0.122	0.81	0.125	0.27	0.27	0.278	0.261
S420MC	3	469	587	0.129	0.82	0.127	0.279	0.32	0.327	0.338
S420MC	3.5	483	592	0.117	0.73	0.129	0.282	0.34	0.343	0.339
S420MC	5	477	606	0.116	0.76	0.127	0.301	0.37	0.396	0.417
QStE460TM	2	497	623	0.103	0.78	0.115	0.253	0.26	0.261	0.224
QStE460TM	2.5	483	603	0.107	0.82	0.116	0.254	0.28	0.283	0.260
QStE460TM	3.6	491	611	0.11	0.74	0.112	0.263	0.3	0.321	0.327
QStE500TM	1.8	544	619	0.097	0.82	0.101	0.227	0.22	0.227	0.202
QStE500TM	2.5	565	636	0.098	0.83	0.109	0.237	0.27	0.266	0.241
QStE500TM	3	551	659	0.096	0.78	0.108	0.232	0.29	0.275	0.262
QStE500TM	4.5	542	643	0.102	0.84	0.112	0.248	0.31	0.318	0.351
QStE500TM	6	553	632	0.103	0.81	0.116	0.252	0.32	0.341	0.424
QStE550TM	2	574	665	0.09	0.8	0.098	0.216	0.23	0.230	0.199
QStE550TM	2.5	595	687	0.091	0.76	0.123	0.211	0.26	0.245	0.225
QStE550TM	2.8	604	690	0.085	0.82	0.112	0.219	0.27	0.259	0.226
QStE550TM	3	587	682	0.082	0.86	0.104	0.221	0.275	0.265	0.227
QStE550TM	3.5	591	664	0.089	0.79	0.109	0.231	0.29	0.284	0.268
QStE600TM	2	633	732	0.079	0.78	0.094	0.207	0.22	0.225	0.176
QStE600TM	2.5	635	738	0.08	0.86	0.096	0.208	0.24	0.243	0.201
QStE600TM	3.5	622	716	0.081	0.85	0.095	0.212	0.26	0.268	0.246
QStE600TM	5	627	727	0.072	0.81	0.103	0.21	0.28	0.287	0.265
QStE650TM	2	674	790	0.068	0.77	0.091	0.19	0.22	0.217	0.154
QStE650TM	2.5	665	782	0.066	0.82	0.092	0.196	0.24	0.237	0.173
QStE650TM	3	661	776	0.070	0.83	0.095	0.205	0.25	0.254	0.197
QStE700TM	1.5	739	804	0.062	0.78	0.082	0.181	0.19	0.178	0.123
QStE700TM	1.8	725	790	0.060	0.83	0.08	0.182	0.195	0.204	0.130
QStE700TM	2	737	802	0.063	0.76	0.084	0.171	0.2	0.212	0.143
QStE700TM	2.5	747	820	0.058	0.8	0.081	0.178	0.23	0.230	0.149
QStE700TM	3	724	796	0.061	0.81	0.086	0.184	0.25	0.244	0.174
QStE700TM	4	732	784	0.062	0.73	0.087	0.204	0.26	0.271	0.211
BR440/580HE	3	514	574	0.168	0.75	0.131	0.277	0.35	0.324	0.421

Table A1. *Cont.*

Steel	t (mm)	Rp (MPa)	Rm (MPa)	n-Value	r-Value	Ag	At	Exp FLC_0	Cal FLC_0	Keeler FLC_0
580DP	3.5	389	636	0.175	0.8	0.175	0.31	0.4	0.380	0.472
700DP	2.5	425	758	0.138	0.76	0.125	0.24	0.27	0.269	0.325
780DP	3.2	577	848	0.125	0.82	0.121	0.21	0.28	0.261	0.341
FB590	2.2	512	621	0.102	0.77	0.128	0.257	0.3	0.275	0.233
FB780	3	665	813	0.071	0.81	0.084	0.187	0.26	0.245	0.200
FB780	4	672	810	0.075	0.75	0.079	0.194	0.29	0.265	0.250
B780NP	3	756	801	0.082	0.88	0.085	0.25	0.3	0.293	0.227
B780NP	3.5	766	812	0.082	0.83	0.091	0.26	0.33	0.316	0.249
B780SF	2.5	784	856	0.080	0.89	0.081	0.245	0.28	0.274	0.201
B510L	3	435	562	0.132	0.9	0.152	0.277	0.33	0.324	0.344
B510L	4	413	535	0.135	0.93	0.155	0.285	0.38	0.357	0.413
B510L	5	420	544	0.136	0.89	0.158	0.294	0.41	0.386	0.474
B510L	6	446	533	0.143	0.69	0.151	0.31	0.41	0.424	0.550
B530L	3	426	562	0.132	0.86	0.148	0.29	0.32	0.341	0.344
B550L	5	480	575	0.125	0.81	0.145	0.278	0.35	0.364	0.443
B610L	3	556	637	0.104	0.82	0.105	0.232	0.28	0.275	0.271
B610L	4.5	572	652	0.103	0.78	0.121	0.24	0.31	0.309	0.354
B650L	3	597	688	0.093	0.83	0.105	0.22	0.26	0.265	0.254
B700L	3	654	732	0.087	0.78	0.106	0.212	0.25	0.259	0.252
B750L	2.5	733	785	0.062	0.77	0.084	0.183	0.23	0.231	0.159
B750L	3.5	735	793	0.064	0.81	0.086	0.184	0.24	0.253	0.200
BWP750	1.5	720	795	0.063	0.75	0.084	0.21	0.22	0.189	0.125
BWP750	3.5	718	804	0.068	0.84	0.096	0.205	0.26	0.263	0.211
BWP750	4	695	805	0.071	0.78	0.092	0.21	0.28	0.275	0.238
B980	2	859	1047	0.06	0.75	0.067	0.14	0.23	0.216	0.137

References

1. Jha, G.; Das, S.; Lodh, A.; Haldar, A. Development of hot rolled steel sheet with 600MPa UTS for automotive wheel application. *Mater. Sci. Eng. A* **2012**, *552*, 457–463. [CrossRef]
2. Hu, J.; Du, L.X.; Wang, J.J.; Sun, Q.Y. Cooling process and mechanical properties design of hot-rolled low carbon high strength microalloyed steel for automotive wheel usage. *Mater. Des.* **2014**, *53*, 332–337. [CrossRef]
3. Chen, W.J.; Song, H.W.; Lazarescu, L.; Xu, Y.; Zhang, S.H.; Banabic, D. Formability analysis of hot-rolled dual-phase steel during the multistage stamping process of wheel disc. *Int. J. Adv. Manuf. Technol.* **2020**, *110*, 1563–1573. [CrossRef]
4. Sansot, P.; Frédéric, B.; Vitoon, U.; Surasak, S.; Suwat, J. Experimental and theoretical formability analysis using strain and stress based forming limit diagram for advanced high strength steels. *Mater. Des.* **2013**, *51*, 756–766.
5. Keeler, S.P.; Backhofen, W.A. Plastic instability and fracture in sheet stretched over rigid punches. *ASM Trans.* **1963**, *56*, 25–48.
6. Marciniak, Z.; Kuczynski, K. Limit strains in the processes of stretch forming sheet metal. *Int. J. Mech. Sci.* **1967**, *9*, 609–612. [CrossRef]
7. Nakazima, K.; Kikuma, T.; Hasaku, K. Study on the formability of steel sheet. *Yawata Technol. Rep.* **1968**, *264*, 8517–8530.
8. Xia, L.L.; Xu, Y.; El-Aty, A.A.; Zhang, S.H.; Nielsen, K.B.; Li, J.M. Deformation characteristics in hydro-mechanical forming process of thin-walled hollow component with large deformation: Experimentation and finite element modeling. *Int. J. Adv. Manuf. Technol.* **2019**, *104*, 4705–4714. [CrossRef]
9. Banabic, D.; Aretz, H.; Paraianu, L.; Jurco, P. Application of various FLD modelling approaches. *Mod. Sim. Mater. Sci. Eng.* **2005**, *13*, 759–769. [CrossRef]
10. Ma, Y.; Chen, S.F.; Chen, D.Y.; Banabic, D.; Song, H.W.; Xu, Y.; Zhang, S.H.; Fan, X.S.; Wang, Q. Determination of the forming limit of impact hydroforming by frictionless full zone hydraulic forming test. *Int. J. Mater. Form.* **2021**, *14*, 1221–1232. [CrossRef]
11. Kasaei, M.M.; Oliveira, M.C. Influence of the contact with friction on the deformation behavior of advanced high strength steels in the Nakajima test. *J. Strain Anal. Eng.* **2022**, *57*, 193–207. [CrossRef]
12. Banabic, D.; Lazarescu, L.; Paraianu, L.; Ciobanu, I.; Nicodim, I.; Comsa, D.S. Development of a new procedure for the experimental determination of the Forming Limit Curves. *Ann. CIRP* **2013**, *62*, 255–258. [CrossRef]
13. Yang, Q.B.; Min, J.Y.; Carsley, J.E.; Wen, Y.Y.; Kuhlenkötter, B.; Stoughton, T.B.; Lin, J.P. Prediction of plane-strain specimen geometry to efficiently obtain a forming limit diagram by Marciniak test. *J. Iron Steel Res. Int.* **2018**, *25*, 539–545. [CrossRef]
14. Holmberg, S.; Enquist, B.; Thilderkvist, P. Evaluation of sheet metal formability by tensile tests. *J. Mater. Process Technol.* **2004**, *145*, 72–83. [CrossRef]
15. Swift, H.W. Plastic instability under plane stress. *J. Mech. Phys. Solids* **1952**, *1*, 1–18. [CrossRef]
16. Hill, R. On discontinuous plastic states with special reference to localized necking in thin sheets. *J. Mech. Phys. Solids.* **1952**, *1*, 19–30. [CrossRef]
17. Bleck, W.; Deng, Z.; Papamantellos, K.; Gusek, C.O. A comparative study of the forming limit diagram models for sheet steels. *J. Mater. Process Technol.* **1998**, *83*, 223–230. [CrossRef]

18. Banabic, D.; Kami, A.; Comsa, D.S.; Eyckens, P. Developments of the Marciniak-Kuczynski model for sheet metal formability: A review. *J. Mater. Process Technol.* **2021**, *287*, 116446. [CrossRef]
19. Hao, Q.G.; Qin, S.W.; Liu, Y.; Zuo, X.W.; Chen, N.L.; Rong, Y.H. Relation between microstructure and formability of quenching-partitioning-tempering martensitic steel. *Mater. Sci. Eng. A* **2016**, *671*, 135–146. [CrossRef]
20. Chen, W.J.; Yin, S.; Pei, X.H. Mechanical property and formability of 580DP and 700DP hot-rolled dual phase steel. *Mater. Mech. Eng.* **2020**, *44*, 92–97.
21. Ma, B.L.; Wan, M.; Zhang, H.; Gong, X.L.; Wu, X.D. Evaluation of the forming limit curve of medium steel plate based on non-constant through-thickness normal stress. *J. Manuf. Process.* **2018**, *33*, 175–183. [CrossRef]
22. Kim, W.; Koh, Y.; Kim, H. Formability evaluation for hot-rolled HB780 steel sheet based on 3-D non-quadratic yield function. *Met. Mater. Int.* **2017**, *23*, 519–531. [CrossRef]
23. Sing, W.M.; Rao, K.P. Prediction of sheet-metal formability using tensile-test results. *J. Mater. Process Technol.* **1993**, *37*, 37–51. [CrossRef]
24. Keeler, S.P.; Brazier, S.G. Relationship between laboratory material characterization and press-shop formability. *Proc. Microalloying* **1977**, *75*, 517–530.
25. Raghavan, K.S.; Van Kuren, R.C.; Darlington, H. Recent progress in the development of forming limit curves for automotive sheet steel. *SAE Technol. Pap.* **1992**, 920437. [CrossRef]
26. Paul, S.K. Prediction of complete forming limit diagram from tensile properties of various steel sheets by a nonlinear regression based approach. *J. Manuf. Process.* **2016**, *23*, 192–200. [CrossRef]
27. Paul, S.K.; Manikandan, G.; Verma, R.K. Prediction of entire forming limit diagram from simple tensile material properties. *J. Strain Anal. Eng.* **2013**, *48*, 386–394. [CrossRef]
28. Cayssials, F. A new method for predicting FLC. In Proceedings of the 20th IDDRG Congress, Brussels, Belgium, 17–19 June 1998; pp. 443–454.
29. Cayssials, F.; Lemoine, X. Predictive model for FLC (arcelor model) upgraded to UHSS steels. In Proceedings of the 24th IDDRG Conference, Besançon, France, 20–22 June 2005; pp. 17.1–17.8.
30. Abspoel, M.; Scholting, M.E.; Droog, J.M.M. A new method for predicting forming limit curves from mechanical properties. *J. Mater. Process Technol.* **2013**, *213*, 759–769. [CrossRef]
31. Abspoel, M.; Scholting, M.E.; Lansbergen, M.; An, Y.; Vegter, H. A new method for predicting advanced yield criteria input parameters from mechanical properties. *J. Mater. Process Technol.* **2017**, *248*, 161–177. [CrossRef]
32. Gerlach, J.; Kessler, L.; Kohler, A. The forming limit curve as a measure of formability is an increase of testing necessary for robustness simulations. In Proceedings of the IDDRG 50th Anniversary Conference, Graz, Austria, 31 May–2 June 2010; pp. 479–488.
33. Gerlach, J.; Kessler, L.; Kohler, A.; Paul, U. Method for the approximate calculation of forming limit curves using tensile test results. *Stahl. Und Eisen* **2010**, *130*, 55–61.
34. Pimentel, A.M.F.; de Carvalho Martins Alves, J.L.; de Seabra Merendeiro, N.M.; Vieira, D.M.F. Comprehensive benchmark study of commercial sheet metal forming simulation softwares used in the automotive industry. *Int. J. Mater. Form.* **2018**, *11*, 879–899. [CrossRef]
35. *ISO 6892-1:2019*; Metallic Materials—Tensile Testing—Part 1: Method of Test at Room Temperature. ISO: Geneva, Switzerland, 2019.
36. *ISO 10113:2020*; Metallic Materials—Sheet and Strip—Determination of Plastic Strain Ratio. ISO: Geneva, Switzerland, 2020.
37. *ISO 10275:2020*; Metallic Materials—Sheet and Strip—Determination of Tensile Strain Hardening Exponent. ISO: Geneva, Switzerland, 2020.
38. *ISO 12004-2: 2008*; Metallic Materials—Sheet and Strip—Determination of Forming-Limit Curves—Part 2: Determination of Forming-Limit Curves in Laboratory. ISO: Geneva, Switzerland, 2008.
39. Shi, M.F.; Gelisse, S. Issues on the AHSS forming limit determination. In Proceedings of the 25th IDDRG Conference, Porto, Portugal, 19–21 June 2006; pp. 19–25.
40. Ghazanfari, A.; Assempour, A. Calibration of forming limit diagrams using a modified Marciniak–Kuczynski model and an empirical law. *Mater. Des.* **2012**, *34*, 185–191. [CrossRef]
41. Chezan, A.R.; Khandeparkar, T.V.; ten Horn, C.H.L.J.; Sigvant, M. Accurate sheet metal forming modeling for cost effective automotive part production. In Proceedings of the 38th IDDRG Conference, Enschede, The Netherlands, 3–7 June 2019; Volume 651, p. 012007.
42. Yun, X.; Gardner, L. Stress-strain curves for hot-rolled steels. *J. Constr. Steel Res.* **2017**, *133*, 36–46. [CrossRef]
43. Hosford, W.F.; Duncan, J.L. Sheet metal forming: A review. *JOM* **1999**, *51*, 39–44. [CrossRef]
44. Hashemi, R.; Ghazanfari, A.; Abrinia, K.; Assempour, A. The effect of the imposed boundary rate on the formability of strain rate sensitive sheets using the M-K method. *J. Mater. Eng. Perform.* **2013**, *22*, 2522–2527. [CrossRef]
45. Keeler, S.P. Forming limit criteria sheets. In *Advances in Deformation Processing*; Burke, J.J., Weiss, V., Eds.; Plenum Press: New York, NY, USA, 1989; pp. 127–157.

46. Levy, B.S.; Van Tyne, C.J. An approach to predicting the forming limit stress components from mechanical properties. *J. Mater. Process Technol.* **2016**, *229*, 758–768. [CrossRef]
47. Lu, W.Q.; Chen, J.S.; Chen, J.; Shi, L.; Xiao, H.; Tong, G. Application of minimum thickness criterion in forecasting FLC of high-strength hot rolled-sheet metal. *Mater. Sci. Technol.* **2010**, *18*, 387–395.